Impact of substrate temperature on the structural and optical properties of strain-balanced InAs/InAsSb type-II superlattices grown by molecular beam epitaxy

Shi Liu, Hua Li, Oray O. Cellek, Ding Ding, Xiao-Meng Shen, Zhi-Yuan Lin, Elizabeth H. Steenbergen, Jin Fan, Zhao-Yu He, Jing Lu, Shane R. Johnson, David J. Smith, and Yong-Hang Zhang

Citation: Applied Physics Letters **102**, 071903 (2013); doi: 10.1063/1.4793231
View online: http://dx.doi.org/10.1063/1.4793231
View Table of Contents: http://scitation.aip.org/content/aip/journal/apl/102/7?ver=pdfcov
Published by the AIP Publishing

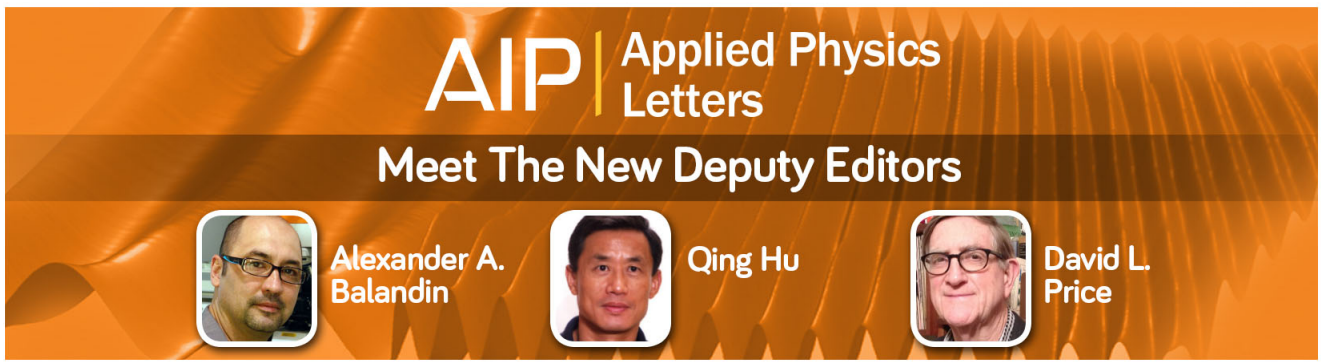

Impact of substrate temperature on the structural and optical properties of strain-balanced InAs/InAsSb type-II superlattices grown by molecular beam epitaxy

Shi Liu,[1,2] Hua Li,[1,2] Oray O. Cellek,[1,2] Ding Ding,[1,2] Xiao-Meng Shen,[2,3] Zhi-Yuan Lin,[1,2] Elizabeth H. Steenbergen,[1,2] Jin Fan,[2,4] Zhao-Yu He,[1,2] Jing Lu,[3] Shane R. Johnson,[1,2] David J. Smith,[2,4] and Yong-Hang Zhang[1,2,a)]

[1]*School of Electrical, Computer and Energy Engineering, Arizona State University, Tempe, Arizona 85287, USA*
[2]*Center for Photonics Innovation, Arizona State University, Tempe, Arizona 85287, USA*
[3]*School for Engineering of Matter, Transport and Energy, Arizona State University, Tempe, Arizona 85287, USA*
[4]*Department of Physics, Arizona State University, Tempe, Arizona 85287, USA*

(Received 24 January 2013; accepted 7 February 2013; published online 20 February 2013)

Molecular beam epitaxial growth of strain-balanced InAs/$InAs_{1-x}Sb_x$ type-II superlattices on GaSb substrates has been investigated for substrate temperatures from 400 °C to 450 °C. The Sb composition is found to vary linearly with substrate temperature at constant V/III ratios. For samples grown at the optimized substrate temperature (410 °C), superlattice zero-order peak full-width at half-maximums are routinely less than 25 arc sec using high-resolution X-ray diffraction. Cross-sectional transmission electron microscopy images show the absence of any visible defects. Strong photoluminescence covers a wavelength range from 5.5 to 13 μm at 12 K. Photoluminescence linewidth simulations show satisfactory agreement with experiments. © *2013 American Institute of Physics*. [http://dx.doi.org/10.1063/1.4793231]

Type-II superlattices (T2SLs) were initially proposed several decades ago,[1,2] and they have been extensively studied as possible alternatives to mercury cadmium telluride (MCT) for infrared (IR) detector applications.[3,4] Great efforts have been expended towards developing state-of-the-art InAs/Ga(In)Sb IR detectors.[5–10] However, the minority carrier lifetimes are still more than an order of magnitude shorter than those of MCT.[11,12] The native defects present in GaSb bulk or superlattice (SL) materials have been identified to be non-radiative recombination centers responsible for the limited lifetimes.[13] In parallel to the study of InAs/Ga(In)Sb SLs, Ga-free type-II material systems, such as In(As)Sb/InAsSb,[14,15] or InAs/InAsSb,[16] have been studied, and the latter, InAs/InAsSb SLs, were also grown strain-balanced on GaSb substrates with much thicker layers and low defect density.[17] A recent time-resolved photoluminescence study of InAs/$InAs_{1-x}Sb_x$ SLs has demonstrated a minority carrier lifetime of over 500 ns,[18,19] much longer than that (~30 ns) achieved with InAs/GaSb SLs, offering great potential for device applications.

Molecular beam epitaxial (MBE) growth of $InAs_{1-x}Sb_x$ alloys over the entire composition range has been studied using InSb, GaAs,[15] and InAs[20] substrates. Photoluminescence (PL) emission was observed for wavelengths as long as 8 μm at 10 K for $x = 0.72$.[21] However, this composition is not ideal for long-wave infrared (LWIR) detectors due to the large lattice mismatch to the available III-V substrates (4.3% to GaSb, −1.8% to InSb). It was also reported that there is a large miscibility gap for $InAs_{1-x}Sb_x$ alloys (from $x = 0.065$ to 0.65 at 400 °C),[22] and spontaneous phase separation was reported in $InAs_{0.50}Sb_{0.50}$ MBE layers grown below 430 °C.[23] Meanwhile, Sb surface segregation on InAs overlayers and As-for-Sb exchange in GaSb underlayers were reported at InAs/GaSb interfaces.[24] The same effects are expected to take place at InAs/$InAs_{1-x}Sb_x$ interfaces, but Sb segregation can be suppressed more effectively at these interfaces because of the relatively low Sb/III ratio used during growth. The Sb incorporation rate in $InAs_{1-x}Sb_x$ was shown to be sensitive to the substrate temperature (300 °C ~ 480 °C), especially at high Sb beam flux,[15,25] but the influence of the substrate temperature has not yet been thoroughly investigated for InAs/$InAs_{1-x}Sb_x$ SL structures with a type-II band alignment. Hitherto, there have only been a few reports in the literature on the growth of strain-balanced InAs/$InAs_{1-x}Sb_x$ SL structures, which were carried out using both metalorganic chemical vapor deposition (MOCVD)[26–29] and MBE.[17,30,31]

In the present work, we have investigated the impact of growth temperature on the structural quality and optical properties of InAs/$InAs_{1-x}Sb_x$ T2SLs grown by solid-source MBE and demonstrated the realization of IR emission longer than 12 μm at 10 K. The V/III flux ratios are kept constant at 1.2 and 1.0 for As/In and Sb/In, respectively, and the growth rate of InAs is fixed at 9.15 nm/min or 0.5 ML/s. Details of the materials growth and characterization procedures have been described elsewhere.[31] For each sample, a 500-nm-thick GaSb buffer layer is grown preceding the growth of the InAs/$InAs_{1-x}Sb_x$ SL, which is sandwiched by 10-nm-thick AlSb barrier layers. A 10-nm-thick GaSb layer is grown on top of the second AlSb barrier layer as a capping layer. The key parameters of the sample structures, growth conditions, and X-ray diffraction (XRD) results are summarized in Table I.

The samples studied here are divided into two groups. In group I, the substrate temperature is varied with all other conditions kept the same. In group II, the substrate

a)Electronic mail: yhzhang@asu.edu.

TABLE I. Structures, growth conditions, and XRD results of various InAs/$InAs_{1-x}Sb_x$ samples; x is the Sb composition and $\Delta a/a$ is the lattice mismatch.

			Design			XRD results			
Group	Sample	T_{sub} (°C)	d_{InAsSb} (nm)	d_{InAs} (nm)	Period repeat number	$d_{SL} \pm 0.1$ (nm)	$x \pm 0.01$	$\Delta a/a$	FWHM (arc sec)
I	A	450	2.50	8.10	91	10.5	0.26	-2.0×10^{-3}	38
	B	440	2.50	8.10	91	10.3	0.27	-1.9×10^{-3}	38
	C	420	2.50	8.10	91	10.9	0.34	-6.5×10^{-4}	29
	D	400	2.50	8.10	91	11.0	0.39	9.0×10^{-6}	29
II	E	410	2.83	9.17	91	12.1	0.36	-5.3×10^{-4}	25
	F	410	4.70	15.3	48	19.9	0.35	-9.1×10^{-4}	22
	G	410	5.80	18.8	39	24.4	0.36	-5.3×10^{-4}	22

temperature is kept fixed, while the SL periods are adjusted to obtain longer PL emission wavelengths. The total SL thickness of all the samples is designed to be 1 μm so that the integrated PL intensities can be compared to investigate the impact of defect densities on optical properties. The investigated substrate temperatures of the SLs are 400 °C to 450 °C (samples A to D), and at the optimized substrate temperature of 410 °C, the SL periods are then varied from 12.0 nm to 24.6 nm (samples E, F, and G). The thickness ratios between InAs and $InAs_{1-x}Sb_x$ are kept at 3.24, while the target Sb composition of the $InAs_{1-x}Sb_x$ layers is $x = 0.39$ in order to achieve full strain compensation, as well as a large wavefunction overlap for LWIR emission. According to our previous calculations,[30] larger wavefunction overlaps can be obtained in strain-balanced structures by increasing the Sb composition of the $InAs_{1-x}Sb_x$ layer and decreasing the SL period thickness. Nevertheless, the best structural quality of the $InAs_{1-x}Sb_x$ layers can only be assured within a small substrate temperature window, and the highest Sb composition is necessarily limited by the As/In ratio, which cannot be lower than 1.0 when growing an InAs layer. Thus, the Sb composition chosen here is a compromise between material quality and wavefunction overlap.

The grown SL structures are characterized by high-resolution XRD. Fig. 1 shows two examples of (004) $\omega-2\theta$ profiles and simulations for samples E and G, which have different SL periods. These two samples, especially sample G, have relatively large SL periods, which result in envelope modulation of the satellite peaks on both sides of the substrate peak, corresponding to $InAs_{1-x}Sb_x$ on the left and InAs on the right, respectively. Hence, the zeroth-order SL peak no longer has the highest intensity compared with those of the satellite peaks and has to be determined using simulation. The average SL periods for all of the samples are also derived from the (004) scans, as shown in Table I. The fluctuations of the SL periods are controlled within ±3.8%. The (113) $\omega-2\theta$ scans are performed subsequently to obtain the overall in-plane lattice mismatch, as well as the average Sb composition of the $InAs_{1-x}Sb_x$ layers. Table I also shows that the lattice mismatch of the 1-μm-thick samples barely exceed 1.0×10^{-3}. The target Sb compositions of the $InAs_{1-x}Sb_x$ layers have been achieved with an error below 3% and proved to be highly reproducible for different SL structures, which is remarkable for a ternary alloy with two group-V elements.

The full-width at half-maximums (FWHM) of the zeroth-order XRD peaks of these SL samples are considered as good indicators of the overall material quality and are also included in Table I. The material quality improves as the substrate temperature decreases from 450 °C, and the lowest FWHMs are observed for the samples grown at 410 °C. The average lattice mismatch of each sample indicates that the sample grown at 400 °C (sample D) reaches the smallest lattice mismatch; however, its FWHM is not as small as those of the samples grown at 410 °C (group II). This is possibly due to the 2.1% lattice mismatch between GaSb (assuming the InAs layers are fully strained on GaSb) and $InAs_{0.61}Sb_{0.39}$. Sample G has a FWHM of the zeroth-order SL peak of 22 arc sec relative to that of the substrate at 19 arc sec, and its cross-sectional transmission electron microscopy (TEM) image (Fig. 2) shows excellent structural quality without any sign of defects, as well as very sharp SL interfaces.

The Sb compositions in the $InAs_{1-x}Sb_x$ layers are plotted versus substrate temperature in Fig. 3. The Sb incorporation rate increased linearly from 26% to 39% as the temperature was decreased from 450 °C to 400 °C, which can be explained by the trends of the As and Sb sticking coefficients. Since the bond energy of InSb is much weaker

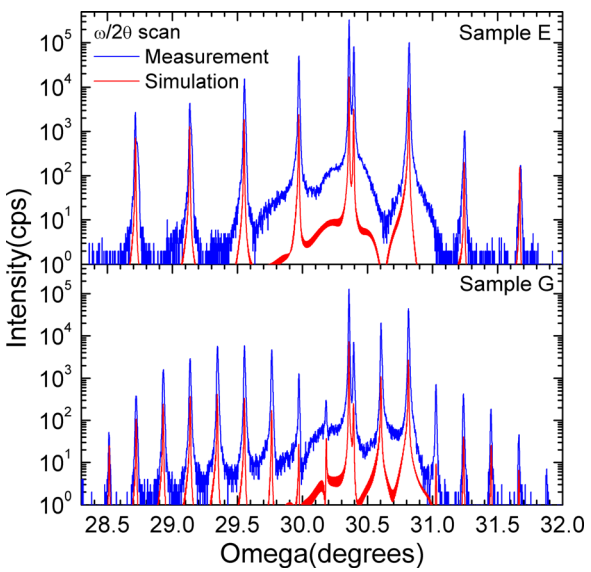

FIG. 1. High-resolution (004) x-ray diffraction patterns and simulations for samples E and G, which are 1-μm thick and have SL periods of 12 and 24.6 nm, respectively.

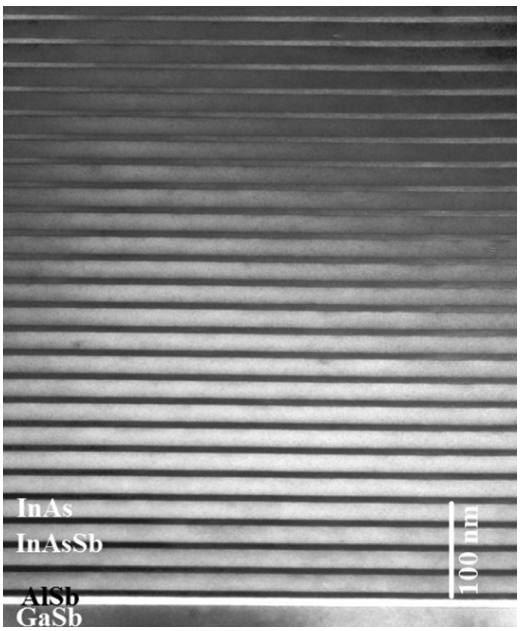

FIG. 2. Cross-section electron micrograph of sample G, demonstrating excellent structural quality.

than that of InAs, it is expected that the As incorporation ratio is much higher than that of Sb for a relatively high substrate temperature. However, as the substrate temperature decreases, the sticking coefficient of Sb increases drastically and approaches a value of unity at some temperature.[32] On the other hand, the sticking coefficient of As increases gradually with decreased substrate temperature and saturates at a value of 0.75.[33] Thus, it is expected that one will get increased Sb composition at lower substrate temperatures with constant V/III ratios, resulting in longer emission wavelength or larger wavefunction overlap.

Figs. 4(a) and 4(b) present the PL spectra of the samples in groups I and II, respectively. For group I, the substrate temperature is denoted beside each peak. Lowered substrate temperature leads to higher Sb composition in the $InAs_{1-x}Sb_x$ layers and thus larger type-II valence band offsets between InAs and $InAs_{1-x}Sb_x$, which gives smaller transition energies in the type-II band alignment. In order to achieve LWIR

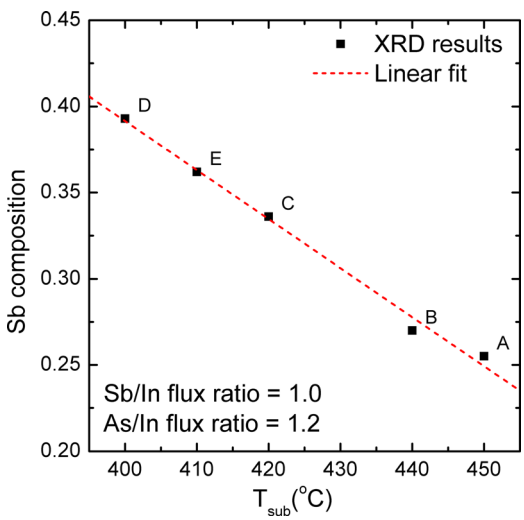

FIG. 3. Sb composition as a function of substrate temperature. The squares are samples A to E and the dotted line is a linear fit.

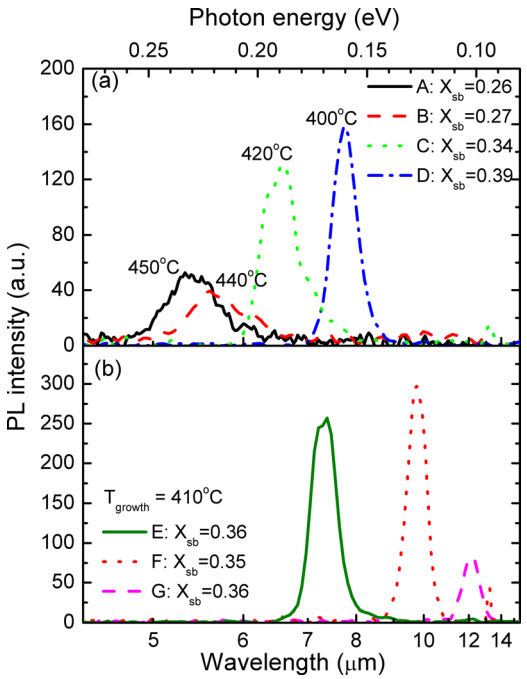

FIG. 4. Low-temperature PL spectra at 12 K for two groups of InAs/$InAs_{1-x}Sb_x$ SL samples: (a) group I and (b) group II.

emission, the substrate temperatures of the group II samples were fixed at 410 °C because the PL peak intensities of samples C and D are much higher than those of A and B. Thicker SL periods are applied to samples E, F, and G as shown in the lower figure, and a PL peak wavelength longer than 12 μm is realized in sample G. Although the PL intensity of sample G is relatively low due to the reduced wavefunction overlap between electrons and holes in the thicker T2SL periods, there is still some margin to increase the period and get emission at even longer wavelengths.

Both the simulated and measured PL linewidths are plotted as a function of the SL periods in Fig. 5. The PL linewidths are attributed to Sb composition fluctuations in the $InAs_{1-x}Sb_x$ layers and InAs/$InAs_{1-x}Sb_x$ interface roughness. Depending on growth conditions, there will be localized fluctuations of InAs and $InAs_{1-x}Sb_x$ layer thicknesses, resulting in InAs or $InAs_{1-x}Sb_x$ islands at the interface. We assume

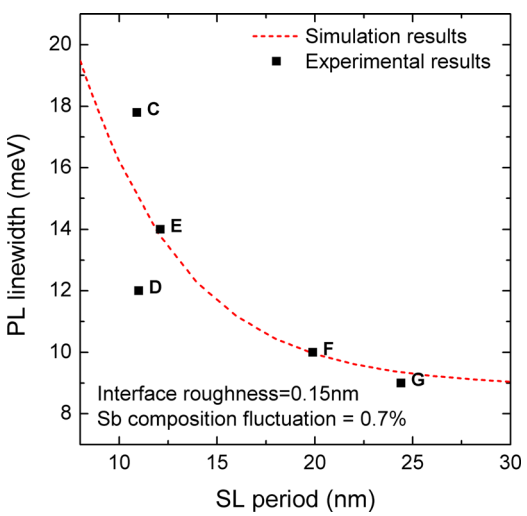

FIG. 5. Simulated and experimental PL linewidth versus SL period.

the height of the islands obeys a Gaussian distribution, and its standard deviation is defined as the interface roughness. We also simply assume equal coverage of InAs and $InAs_{1-x}Sb_x$ islands so that the integrated Sb in the InAs layer equals the integrated extra As in the $InAs_{1-x}Sb_x$ layer. The Sb composition in $InAs_{1-x}Sb_x$ alloy is set at 35% with the fluctuation fixed at 0.7% and the interface roughness fixed at 0.15 nm, in which case the simulation provides the most satisfactory agreement with the experimental data. The result clearly shows that samples with longer SL periods exhibit narrower PL linewidths as the ratio of interface roughness to period decreases, resulting in a relatively smaller fluctuation in the SL period and ground state transition energy.

In summary, we have studied the MBE growth of strain-balanced InAs/$InAs_{1-x}Sb_x$ T2SLs on GaSb (100) substrates at different substrate temperatures. Well-controlled structural properties and SL layer thicknesses were confirmed by high-resolution XRD measurements and TEM images. Lattice mismatches of less than 5×10^{-4} were achieved for the 1-μm-thick T2SL structures. The Sb composition in the $InAs_{1-x}Sb_x$ layers was obtained via symmetric and asymmetric XRD scans, and its relationship with the substrate temperature was investigated. In addition, low temperature PL measurements were performed. The strongest PL intensity was observed from the samples grown at 410 °C, which was then selected as the optimal substrate temperature and used to demonstrate T2SL structures with LWIR emissions beyond 12 μm.

The authors are grateful for the support of ARO MURI program W911NF-10-1-0524 (administered by U.S. Army Research Office and monitored by William W. Clark) and an AFOSR Grant (FA9550-10-1-0129 monitored by Dr. Kitt Reinhardt), and they gratefully acknowledge use of facilities in the John M. Cowley Center for High Resolution Electron Microscopy and LeRoy Eyring Center for Solid State Science at Arizona State University.

[1]L. Esaki and R. Tsu, IBM J. Res. Dev. **14**, 61 (1970).
[2]G. Sai-Halasz, R. Tsu, and L. Esaki, Appl. Phys. Lett. **30**, 651 (1977).
[3]D. L. Smith and C. Mailhot, J. Appl. Phys. **62**, 2545 (1987).
[4]P. M. Young, C. H. Grein, H. Ehrenreich, and R. H. Miles, J. Appl. Phys. **74**, 4774 (1993).
[5]S. B. Rafol, A. Soibel, A. Khoshakhlagh, J. Nguyen, J. K. Liu, J. M. Mumolo, S. A. Keo, L. Hoglund, D. Z. Ting, and S. D. Gunapala, IEEE J. Quantum Electron. **48**, 878 (2012).
[6]M. Sundaram, A. Reisinger, R. Dennis, K. Patnaude, D. Burrows, J. Bundas, K. Beech, and R. Faska, Infrared Phys. Technol. **54**, 243 (2011).
[7]M. Razeghi, D. Hoffman, B.-M. Nguyen, P.-Y. Delaunay, E. K.-W. Huang, M. Z. Tidrow, and V. Nathan, Proc. IEEE **97**, 1056 (2009).
[8]H. S. Kim, E. Plis, J. B. Rodriguez, G. D. Bishop, Y. D. Sharma, L. R. Dawson, S. Krishna, J. Bundas, R. Cook, D. Burrows, R. Dennis, K. Patnaude, A. Reisinger, and M. Sundaram, Appl. Phys. Lett. **92**, 183502 (2008).
[9]R. Rehm, M. Walther, J. Schmitz, J. Fleissner, F. Fuchs, J. Ziegler, and W. Cabanski, Opto-Electron. Rev. **14**, 19 (2006).
[10]I. Vurgaftman, C. L. Canedy, E. M. Jackson, J. A. Nolde, C. A. Affouda, E. H. Aifer, J. R. Meyer, A. Hood, A. J. Evans, and W. T. Tennant, Opt. Eng. **50**, 061007 (2011).
[11]B. C. Connelly, G. D. Metcalfe, H. Shen, and M. Wraback, Appl. Phys. Lett. **97**, 251117 (2010).
[12]D. Donetsky, G. Belenky, S. Svensson, and S. Suchalkin, Appl. Phys. Lett. **97**, 052108 (2010).
[13]S. P. Svensson, D. Donetsky, D. Wang, H. Hier, F. J. Crowne, and G. Belenky, J. Cryst. Growth **334**, 103 (2011).
[14]G. C. Osbourn, J. Vac. Sci. Technol. B **2**, 176 (1984).
[15]G. S. Lee, Y. Lo, Y. F. Lin, S. M. Bedair, and W. D. Laidig, Appl. Phys. Lett. **47**, 1219 (1985).
[16]Y.-H. Zhang, Appl. Phys. Lett. **66**, 118 (1995).
[17]A. Y. Lew, E. T. Yu, and Y.-H. Zhang, J. Vac. Sci. Technol. B **14**, 2940 (1996).
[18]E. H. Steenbergen, B. C. Connelly, G. D. Metcalfe, H. Shen, M. Wraback, D. Lubyshev, Y. Qiu, J. M. Fastenau, A. W. K. Liu, S. Elhamri, O. O. Cellek, and Y.-H. Zhang, Appl. Phys. Lett. **99**, 251110 (2011).
[19]E. H. Steenbergen, B. C. Connelly, G. D. Metcalfe, H. Shen, M. Wraback, D. Lubyshev, Y. Qiu, J. M. Fastenau, A. W. K. Liu, S. Elhamri, O. O. Cellek, and Y.-H. Zhang, Proc. SPIE **8512**, 85120L–1 (2012).
[20]M. Y. Yen, B. F. Levine, C. G. Bethea, K. K. Choi, and A. Y. Cho, Appl. Phys. Lett. **50**, 927 (1987).
[21]M. Y. Yen, R. People, K. W. Wecht, and A. Y. Cho, Appl. Phys. Lett. **52**, 489 (1988).
[22]K. Ishida, T. Nomura, H. Tokunaga, H. Ohtani, and T. Nishizawa, J. Less-Common Met. **155**, 193 (1989).
[23]I. T. Ferguson, A. G. Norman, B. A. Joyce, T. Y. Seong, G. R. Booker, R. H. Thomas, C. C. Phillips, and R. A. Stradling, Appl. Phys. Lett. **59**, 3324 (1991).
[24]M. W. Wang, D. A. Collins, T. C. McGill, R. W. Grant, and R. M. Feenstra, J. Vac. Sci. Technol. B **13**, 1689 (1995).
[25]X. Marcadet, A. Rakovska, I. Prevot, G. Glastre, B. Vinter, and V. Berger, J. Cryst. Growth **227–228**, 609 (2001).
[26]D. Lackner, O. J. Pitts, S. Najmi, P. Sandhu, K. L. Kavanagh, A. Yang, M. Steger, M. L. W. Thewalt, Y. Wang, D. W. McComb, C. R. Bolognesi, and S. P. Watkins, J. Cryst. Growth **311**, 3563 (2009).
[27]Y. Huang, J.-H. Ryou, R. D. Dupuis, V. R. D'Costa, E. H. Steenbergen, J. Fan, Y.-H. Zhang, A. Petschke, M. Mandl, and S.-L. Chuang, J. Cryst. Growth **314**, 92 (2011).
[28]E. H. Steenbergen, Y. Huang, J.-H. Ryou, L. Ouyang, J.-J. Li, D. J. Smith, R. D. Dupuis, and Y.-H. Zhang, Appl. Phys. Lett. **99**, 071111 (2011).
[29]D. Lackner, M. Steger, M. L. W. Thewalt, O. J. Pitts, Y. T. Cherng, S. P. Watkins, E. Plis, and S. Krishna, J. Appl. Phys. **111**, 034507 (2012).
[30]E. H. Steenbergen, K. Nunna, L. Ouyang, B. Ullrich, D. L. Huffaker, D. J. Smith, and Y.-H. Zhang, J. Vac. Sci. Technol. B **30**, 02B107 (2012).
[31]H. Li, S. Liu, O. O. Cellek, D. Ding, X.-M. Shen, E. H. Steenbergen, J. Fan, Z. Lin, Z.-Y. He, Q. Zhang, P. T. Webster, S. R. Johnson, L. Ouyang, D. J. Smith, and Y.-H. Zhang, "A calibration method for group V fluxes and impact of V/III flux ratio on the growth of InAs/InAsSb type-II superlattices by molecular beam epitaxy," J. Cryst. Growth (in press).
[32]S. Baba, H. Horita, and A. Kinbara, J. Appl. Phys. **49**, 3632 (1978).
[33]R. Fernandez, J. Cryst. Growth **116**, 98 (1992).